Evaluation of Thermomechanical Damage in Silicon Carbide/Titanium Composites

J. E. Grady* and B. A. Lerch†
NASA Lewis Research Center, Cleveland, Ohio 44135

Composite specimens of Ti-15V-3A1-3Cr-3Sn matrix reinforced with continuous SCS-6 silicon carbide fibers were tested under a variety of thermal and mechanical loadings. A combined experimental/finite element approach was used to estimate the effective in situ modulus of the matrix material and to evaluate changes in modulus due to the applied loads. Several fiber orientations were tested. The results indicate that the effect of thermal loads on composite stiffness varies with fiber orientation. Applications of this method to test specimens damaged by uniaxial tension, thermal cycling, and isothermal fatigue loadings are used to illustrate that, by monitoring overall structural behavior, changes in stiffness caused by thermomechanical loading can be detected.

Introduction

THE mechanical behavior of composite materials depends on the properties of the fiber and matrix constituents. Because of inhomogeneities due to the addition of the fibers and due to thermal loadings that occur during the fabrication process, the in situ matrix properties of the SiC/Ti-15-3 composite can vary significantly from those of the monolithic matrix.[1] Matrix stiffness properties, as well as the integrity of the fiber/matrix bond, will also change as the composite material deforms under applied mechanical and thermal loads.

In this paper an indirect measurement of the effective in situ matrix modulus is obtained using the results of experimental tests together with finite element analysis of the composite test specimens. The term "effective matrix modulus" is used to account for changes in the measured stiffness of the composite. These changes could be due to a variety of damage modes. In this article, however, all damage will be incorporated into and accounted for by changes in the matrix modulus. The resonant frequencies of the individual specimens are measured by vibration testing. Based on the measured frequencies, the effective modulus of the test specimens is determined by finite element analysis. This indirect measurement technique is applied to each individual test specimen in its original, as-fabricated condition, as well as after a heat treatment, and thermal or mechanical loads are applied. The results therefore show how the effective matrix modulus changes with the different applied loads.

Experimental Procedure

Material Fabrication

The composite was fabricated in a proprietary process in which alternating layers of SiC (SCS-6) fibers and foils of Ti-15V-3Cr-3Sn-3A1 (Ti-15-3) were consolidated. Eight rows of fibers were used, yielding a total composite thickness of approximately 0.08 in. The nominal fiber volume fraction was 34%. Additional microstructural details of the material can be found in Refs. 2 and 3. Several fiber orientations were used in this study, consisting of $[90]_8$, $[\pm 30]_{2s}$, $[\pm 45]_{2s}$, $[0/90]_{2s}$, and $[90/0]_{2s}$. The [0/90] had O-deg plies on the outer surfaces, whereas the [90/0] had 90-deg plies on the outer surfaces. Test specimens, as shown in Fig. 1a, of nominal dimension $6 \times 0.5 \times 0.08$ in. and containing a reduced gauge section were cut from the finished panels. The specimens were heat treated for 24 h at 1292°F in vacuum in an attempt to stabilize the α-β-Ti structure.[3]

Vibration Testing

Test specimens were cantilevered in mechanical grips that clamped 2 in. along one end of the specimen, as shown in Fig. 2. A lightweight (142-mg) accelerometer was attached to the midspan of the specimen by use of a thin layer of MIL-A-46050C cyanoacrylate adhesive. Free vibration response of the cantilevered specimen was recorded digitally on a spectrum analyzer and simultaneously displayed on an oscilloscope, as shown in Fig. 3. Figures 3 and 4 show representative measurements of the vibration response for a typical specimen. Figure 3 shows, as displayed on the oscilloscope, the acceleration response in the time domain to a transient load applied at the

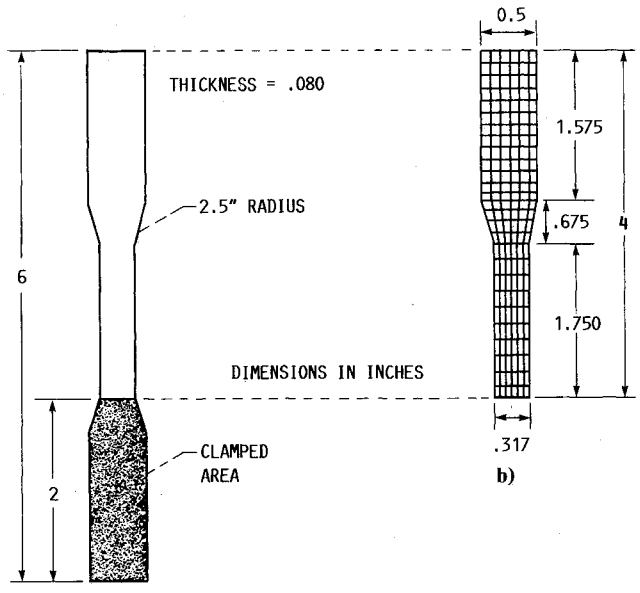

Fig. 1 Test specimen geometry: a) test specimen; b) finite element model.

Presented as Paper 90-1026 at the AIAA/ASME/ASCE/AHS/ASC 31st Structures, Structural Dynamics and Materials Conference, April 2-4, 1990; received Feb. 20, 1990; revision received June 6, 1990; accepted for publication July 5, 1990.

*Research Engineer, 2100 Brookpark Rd., M.S. 49-8. Member AIAA.

†Research Engineer, 2100 Brookpark Rd., M.S. 49-6.

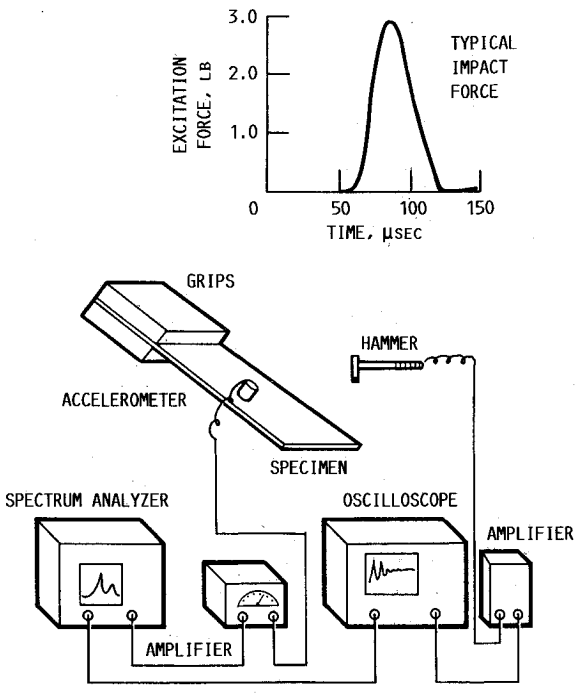

Fig. 2 Experimental apparatus.

free end of the specimen. The corresponding frequency response is shown in Fig. 4. The frequency data were processed using a Hanning window for improved frequency resolution and were obtained by rms averaging for the results of 10 separate tests for each specimen. Resonant frequencies were then identified by digitally locating the peaks in the frequency response signal. Measurements taken in this manner proved to be both extremely sensitive to material changes (e.g., cracking and debonding) caused by the applied loads and repeatable to within a $\pm 0.2\%$ measurement error.

Analysis

Material Properties

Stiffness coefficients for the 8-ply composite test specimens were calculated from the fiber and matrix properties given in Table 1 as follows. For a single unidirectional ply with fibers oriented in the one direction, the elastic constants given by simple rule-of-mixtures calculations are[4]

$$E_{11} = V_f E_f + V_m E_m$$

$$\nu_{12} = V_f \nu_f + V_m \nu_m$$

$$E_{22} = \left[V_f/E_f + V_m/E_m \right]^{-1}$$

$$G_{12} = \left[V_f/G_f + V_m/G_m \right]^{-1}$$

$$\rho = V_f \rho_f + V_m \rho_m \qquad (1)$$

where the subscripts f and m refer to fiber and matrix; E, G, ν, and ρ are the Young's modulus, shear modulus, Poisson's ratio, and mass density, respectively; and V is the volume fraction of the respective constituent. Assuming a state of plane stress in the 1-2 plane, the unidirectional ply stress-strain relations are given by

$$\begin{Bmatrix} \sigma_1 \\ \sigma_2 \\ \sigma_6 \end{Bmatrix} = [Q] \begin{Bmatrix} \epsilon_1 \\ \epsilon_2 \\ \epsilon_6 \end{Bmatrix} \qquad (2)$$

where the subscripts 1 and 2 denote normal in-plane stresses and strains, and 6 denotes in-plane shear. In terms of the engineering constants,

$$[Q] = [S]^{-1}$$

where

$$S_{11} = 1/E_{11} \qquad S_{12} = -\nu_{12}/E_{11}$$

$$S_{22} = 1/E_{22} \qquad S_{13} = S_{23} = 0$$

$$S_{66} = 1/G_{12} \qquad (3)$$

Stress and strain transformation equations are used to calculate $[Q]$ in Eq. (2) for unidirectional ply oriented at an arbitrary angle θ to the 1 direction, and laminated plate theory[5] is then used to calculate membrane and bending stiffness coefficients for the 8-ply composite with arbitrarily oriented plies. These coefficients are then used as the elastic anisotropic constants in the finite element analysis.

The simplifying assumptions inherent in Eqs. (1) are that the fiber/matrix bond is strong and the deformation is elastic. The latter assumption may be adequate in this case since the mod-

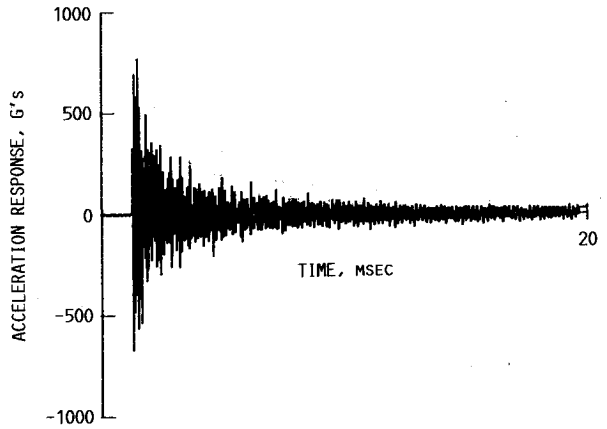

Fig. 3 Accelerometer measurement of free vibration response of specimen 25 after heat treatment.

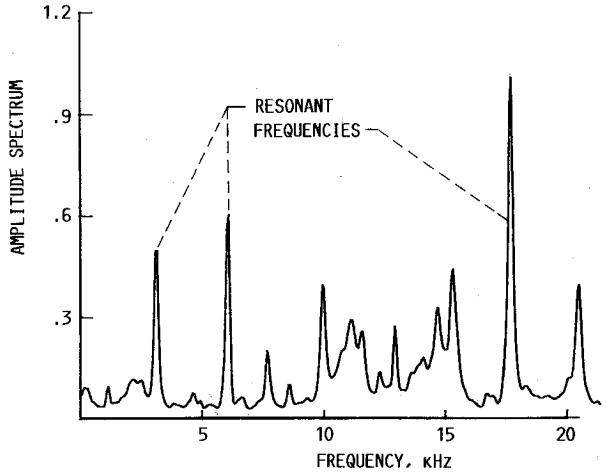

Fig. 4 Amplitude spectrum for specimen 25 after heat treatment.

Table 1 Fiber and matrix elastic properties

	Fiber	Matrix
E, Msi	62	9–15
G, Msi	26	$E/2(1+\nu)$
ν	0.19	0.32
ρ, lb/in.^{3}	0.108	0.172
α, $\times 10^{-6}$/°F	2.7	4.7

Table 2 Specimen 25 $[\pm 30]_{2s}$ frequency data

Vibration mode	As-received condition		
	ω_m[a]	ω_c[b,c]	Percent error
1	— —	181.9	—
2	1 131	1 136	0.4
3	3 190	3 188	0.1
4	6 212	6 274	1.0
5	10 270	10 410	1.4
6	15 300	15 585	1.9

[a]Subscript m, measured value (Hz).
[b]Subscript c, calculated value (Hz).
[c]$E_m = 10.3$ Msi

ulus calculations are being used to predict composite stiffness for small-amplitude vibrations. The actual strength of the fiber/matrix bond is unknown.

Finite Element Analysis

A finite element modal analysis was performed for each test specimen using MSC/NASTRAN.[6] Two-dimensional, isoparametric shell elements with orthotropic membrane and bending stiffness were used to model the composites. Mode shapes and resonant frequencies were calculated by solving the assembled system of equations,

$$\left[[K]-\lambda_i[M]\right]\{\xi_i\}=0 \tag{4}$$

for its eigenvectors and eigenvalues, where

K = structural stiffness matrix

M = mass matrix

λ_i = eigenvalue (ω_i^2)

ξ_i = eigenvector (mode shape)

A representative finite element mesh used to analyze the cantilevered tensile specimen with a reduced gauge section is shown in Fig. 1b.

Results and Discussion

Numerical Convergence

A preliminary study was performed to determine the number of finite elements required for a converged modal solution. The results shown in Figs. 5a and 5b are the natural frequencies measured and calculated for a $[\pm 30]_{2s}$ specimen of dimension $6 \times 1 \times 0.075$ in. These figures indicate that the calculated bending frequencies are sensitive to the number of elements in the longitudinal direction. A converged solution is obtained with 30 longitudinal elements, and these results are given in Table 2. Bending stiffness is underestimated with coarser meshes because reduced integration is used to calculate the element stiffness.[6] Thus, 30 longitudinal elements were used in subsequent calculations.

Vibration Analysis

Vibration tests were performed several times for a few selected specimens to determine the measurement repeatability. The measured values for natural frequencies were found to vary a maximum of 0.2% from one test to another. Shifts in frequency due to applied thermal and mechanical loads were usually on the order of 2–3%; hence, this degree of measurement accuracy was considered acceptable.

The placement of the accelerometer on the specimen, as shown in Fig. 2, was chosen so as to detect the flexural (bending) motion of the specimen rather than the torsional (twisting) motion. Therefore, in the results presented here the frequencies are all associated with bending modes. The lowest frequency range scanned for the specimen used in Fig. 5 was 1–1.2 kHz; thus, no data were taken for the 180-Hz bending mode. The dashed lines are the measured resonant frequencies for each of the modes. The calculated frequencies were determined by varying the matrix modulus from 9 to 15 Msi until the frequencies calculated in the finite element analysis were within 1–2% of the measured values. The matrix modulus giving the best agreement with the measured values for this specimen was 10.3 Msi. The results in Figs. 5a and 5b and Table 2 indicate that the frequencies calculated for the first six bending modes correspond well with the measured values.

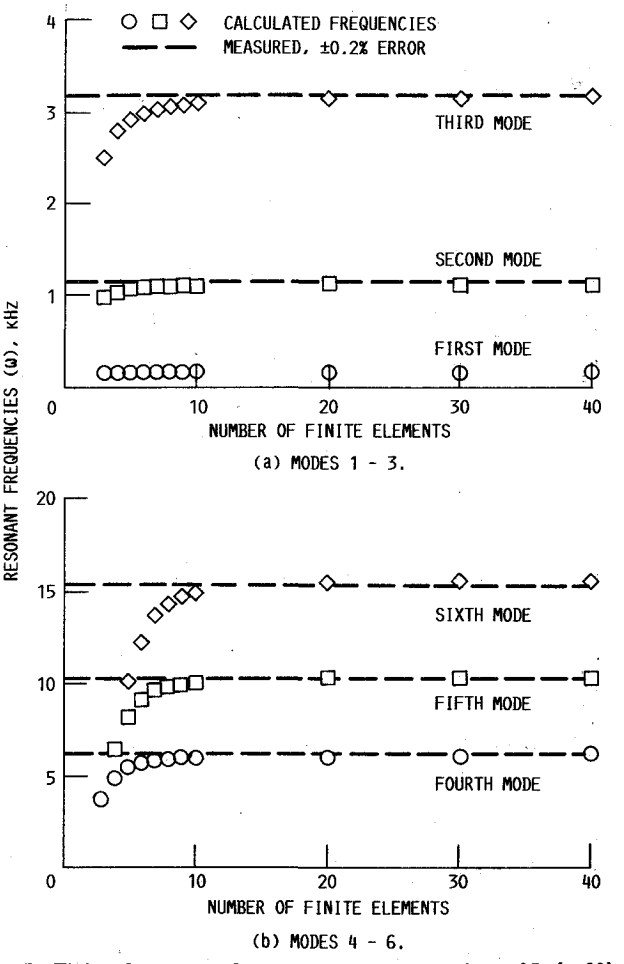

Fig. 5 Finite element mesh convergence: test specimen 25, $[\pm 30]$; matrix modulus: 10.3 Msi.

This procedure was used to determine the effective matrix modulus for each test specimen in the following manner. The matrix modulus used to calculate the finite element stiffness coefficients was systematically varied until the calculated resonant frequencies matched the measured values. This process was repeated three times: to match the measured frequencies of each specimen in its original (as-fabricated) condition, after heat treating, and after a mechanical or thermal load was applied. The effect of each type of loading on the test specimen can therefore be quantified by the change induced in the matrix modulus. An advantage inherent in this combined experimental/finite element approach is that small variations in dimensions between test specimens (e.g., width and thickness variability) are accounted for by minor adjustments in the corresponding dimensions of the finite element model shown in Fig. 1. Therefore, the calculated modulus for one test specimen can be compared directly with that for any other, since the effects of specimen geometry are effectively eliminated.

Heat Treating

In Fig. 6 the effective matrix modulus is presented graphically for each of the ply orientations tested. The average ma-

trix modulus, both before and after heat treating for 24 h at 1292°F in vacuum, is 10.7 Msi. This is somewhat lower than the normal modulus of 12.5 Msi determined from a tensile test for monolithic Ti-15-3 (Ref. 3). The two methods may yield different values. This is currently under investigation. Furthermore, a perfect bond between fiber and matrix has been assumed in the stiffness calculations given in Eqs. (1). Any imperfections in the fiber/matrix bond will lower the composite stiffness and therefore appear as a lower matrix modulus in this model. Similarly, fabrication-induced residual stresses can lead to cracking in the matrix or fiber/matrix interphase region. Both types of damage will lower the effective matrix modulus in these calculations. Nevertheless, the modulus values given here can be used effectively to compare the relative damage states of the different test specimens. The data in Fig. 6 are given in Tables 3–7. Each data point in Fig. 6 represents the results for a single test specimen. However, a series of specimens of each type (i.e., fiber orientation and geometry) was tested. The data shown in each of the figures are representative of the results for the entire series of test specimens. The number of specimens of each type is shown in Table 8.

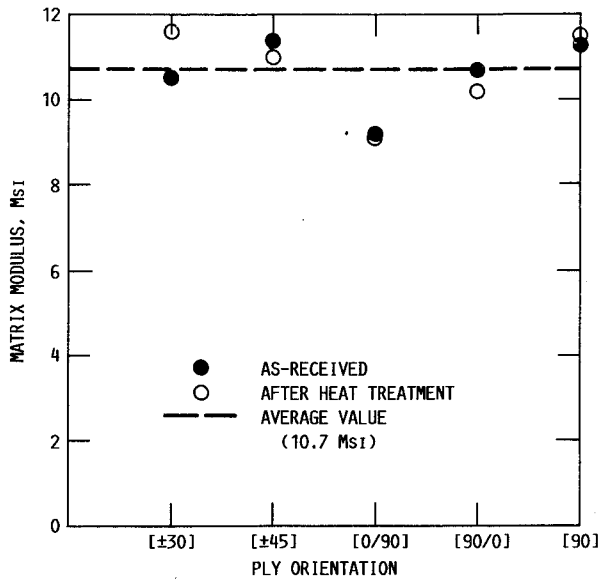

Fig. 6 Calculated matrix modulus before and after 24 h/1292°F heat treatment.

If $\Delta\theta$ is the difference in ply orientation for neighboring plies of the composite, i.e.,

$$\Delta\theta = \theta_i - \theta_{i+1}$$

where the subscript i refers to the ply number, the data in Fig. 6 indicate that heat treatment effectively increased the composite stiffness when $\Delta\theta = 60$ deg or less (i.e., [±30] or [90] fiber orientations) and decreased composite stiffness when $\Delta\theta = 90$ deg (i.e., [±45], [0/90], and [90/0] fiber orientations). These limited data suggest that the response of the composite to heat treatment is dependent on the residual stress state and on the lateral constraining effect that the plies impose on one another.

Tensile tests on monolithic Ti-15-3[3] indicate that, although tensile strength and failure strain are affected by the heat treatment, the elastic modulus is not significantly changed from its original value of approximately 12.5 Msi. Therefore, the changes in effective matrix modulus of the composite caused by heat treating are most likely due to changes in the

Table 3 Specimen 24 $[\pm 30]_{2s}$ frequency data

Vibration mode	As-received condition			After heat treatment[a]			After tensile loading[b]		
	ω_m	ω_c[c]	Percent error	ω_m	ω_c[d]	Percent error	ω_m	ω_c[e]	Percent error
1	— —	183.7	___	— —	188.7	___	— —	182.7	___
2	1 146	1 144	0.15	1 179	1 176	0.25	1 138	1 138	0.02
3	— —	3 215	___	— —	3 304	___	— —	3 199	___
4	6 308	6 325	0.27	6 471	6 498	0.42	6 199	6 292	1.5
5	10 393	10 460	0.64	10 968	10 748	2.0	10 713	10 405	2.9
6	15 435	15 743	2.0	16 260	16 239	0.13	15 705	15 651	0.3

[a]1292°F for 24 h. [b]144 ksi (1.5% strain). [c]$E_m = 10.5$ Msi. [d]$E_m = 11.6$ Msi. [e]$E_m = 10.3$ Msi.
Subscripts m and c as defined in Table 2 footnote.

Table 4 Specimen A1 $[\pm 45]_{2s}$ frequency data

Vibration mode	As-received condition			After heat treatment[a]			After fatigue loading[b]		
	ω_m	ω_c[c]	Percent error	ω_m	ω_c[d]	Percent error	ω_m	ω_c[e]	Percent error
1	___	129.3	___	___	127.4	___	___	126.1	___
2	958.3	958.6	0.03	945.5	945.1	0.04	934.5	935.0	0.05
3	2754	2807	1.9	2722	2768	1.7	2691	2739	1.8
4	5448	5479	0.57	5270	5403	2.5	5280	5346	1.3

[a]1292°F for 24 h. [b]195 LCF cycles at 800°F. [c]$E_m = 11.4$ Msi. [d]$E_m = 11.0$ Msi. [e]$E_m = 10.7$ Msi.
Subscripts m and c as defined in Table 2 footnote.

Table 5 Specimen C1 $[90/0]^{2s}$ frequency data

Vibration mode	As-received condition			After heat treatment[a]			After thermal cycling[b]		
	ω_m	ω_c[c]	Percent error	ω_m	ω_c[d]	Percent error	ω_m	ω_c[e]	Percent error
1	140.0	140.0	0.0	138.0	137.5	0.4	137.5	137.5	0.0
2	1015	1024	0.86	999.0	1006	0.7	1031	1006	2.4
3	2906	2980	2.5	2875	2928	1.8	2969	2928	1.4
4	5659	5798	2.5	5583	5697	2.0	5808	5697	1.9

[a]1292°F for 24 h. [b]2000 cycles: 200–1000°F. [c]$E_m = 10.7$ Msi. [d]$E_m = 10.1$ Msi. [e]$E_m = 10.1$ Msi.
Subscripts m and c as defined in Table 2 footnote.

Table 6 Specimen B7 $[0/90]_{2s}$ frequency data

Vibration	As-received condition			After heat treatment[a]		
	ω_m	ω_c[b]	Percent error	ω_m	ω_c[c]	Percent error
1	151.3	151.4	0.07	150.3	151.1	0.6
2	1102	1107	0.48	1093	1105	1.1
3	3161	3222	1.9	3125	3216	2.9
4	6130	6269	2.3	6081	6257	2.9

[a]1292°F for 24 h. [b]$E_m = 9.2$ Msi. [c]$E_m = 9.1$ Msi.
Subscripts m and c as defined in Table 2 footnote.

Table 7 Specimen 38 $[90]_8$ frequency data

Vibration mode	As-received condition			After heat treatment[a]		
	ω_m	ω_c[b]	Percent error	ω_m	ω_c[c]	Percent error
1	180.5	180.6	0.1	182.0	182.1	0.04
2	___	1319	___	___	1330	___
3	3740	3832	2.4	3800	3863	1.6
4	7210	7479	3.7	7328	7539	2.9

[a]1292°F for 24 h. [b]$E_m = 11.3$ Msi. [c]$E_m = 11.5$ Msi.
Subscripts m and c as defined in Table 2 footnote.

Table 8 Test specimen geometry

Test specimen designation	Fiber orientation	Specimen length	Gauge length	Gauge width	Thickness, in.	Weight, g	No. of specimens
A1	$[\pm 45]_{2s}$	5.980	1.5	0.317	0.076	13.012	10
B7	$[0/90]_{2s}$	5.984	1.5	0.329	0.077	13.374	9
C1	$[90/0]_{2s}$	5.990	1.5	0.329	0.077	13.440	3
24	$[\pm 30]_{2s}$	5.877	⟨a⟩	0.999	0.075	30.105	2
25	$[\pm 30]_{2s}$	5.872	⟨a⟩	0.746	0.075	22.283	2
38	$[90]_8$	5.510	1.0	0.328	0.083	13.765	3

[a]Rectangular specimen.

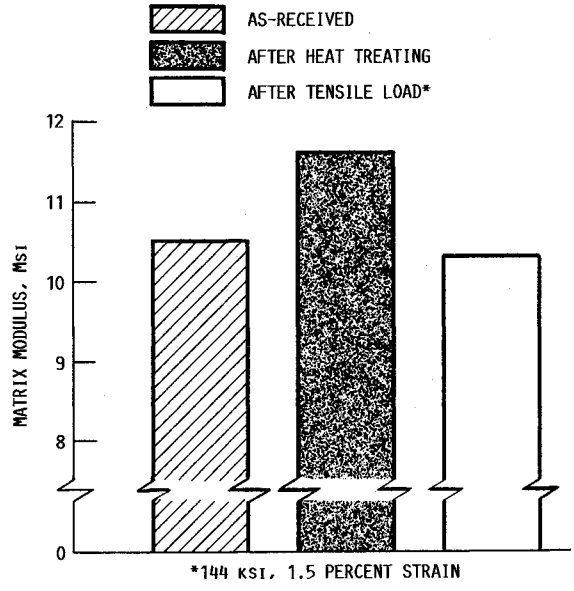

Fig. 7 Change in calculated matrix modulus for [±30] specimen due to heat treatment and tensile load.

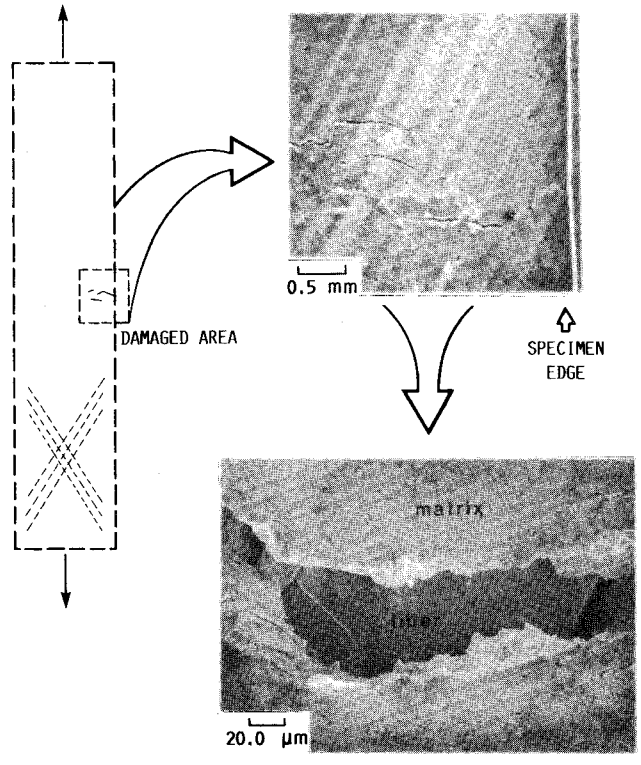

Fig. 8 Scanning electron microscope photographs of damaged area of [±30] specimen loaded in tension to 1.5% strain.

integrity of the fiber/matrix bond that could occur during thermal loading of the composite. The integrity of this bond could be affected by the residual stress state within the individual plies and would therefore vary as a function of the ply stacking sequence. A detailed analysis of the residual stress state is in progress and will be reported subsequently.

Tensile Load

A 144-ksi tensile load was applied to a [±30] specimen after it was heat treated. The test was performed in strain control and at a constant strain rate of $10^{-4}\,s^{-1}$. The maximum strain level reached was 1.5%, which is very close to the failure strain for this fiber orientation. An additional vibration test was performed on the specimen after the tensile load was removed. Effective matrix modulus values were backcalculated, based on the data given in Table 3, and are shown in Fig. 7. The matrix modulus was 11.6 Msi after heat treating but dropped to 10.3 Msi after the tensile load was applied, suggesting that some damage to the composite was caused by the tensile load. Microfocus X-ray analysis was performed on the damaged specimen. This analysis indicated that damage in the form of cracks was concentrated in the area highlighted in Fig. 8. Examination of the damaged area using a scanning electron microscope (SEM) revealed the failure details shown in Fig. 8. As indicated in these micrographs, the outer matrix layer exhibits cracking. The cracking occured on both sides of the specimen in the area indicated by the dashed square. A high magnification of these cracks indicated that the fibers within the crack (i.e., the first fiber row) remained intact. Whether these cracks propagated through the thickness of the specimen is unknown at this time.

Fatigue Load

After heat treatment, a [±45] specimen was fatigue tested at a frequency of 0.1 Hz for 195 tension-tension cycles at 800°F.

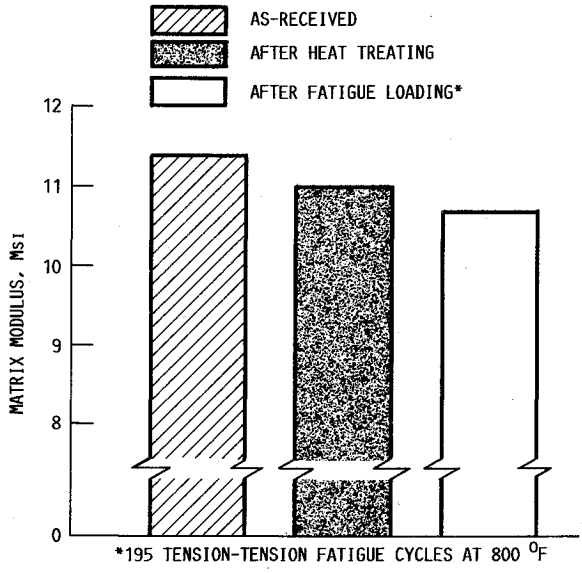

Fig. 9 Change in calculated matrix modulus for [±45] specimen due to heat treatment and fatigue load.

The applied mean stress σ_m was 17.3 ksi, and the stress range $\Delta\sigma$ was 32.9 ksi. The stress ratio $\sigma_{min}/\sigma_{max}$ was therefore 0.05. For these loading conditions 195 cycles is approximately 1% of the expected low cycle fatigue life of the composite.[7] The test data are given in Table 4, and the calculated modulus (10.7 Msi) is compared to the as-received (11.4 Msi) and heat-treated (11.0 Msi) values in Fig. 9. The results indicate that some degradation was caused by the fatigue loading. No metallographic inspection of the damaged specimen has yet been performed; thus, no supporting data are available to identify the type and location of the damage. However, no visible cracking was observed on the outer surfaces of the specimen.

Thermal Cycling

Cyclic thermal loading may cause cracking at or near the fiber/matrix interface region due to the mismatch in thermal expansion coefficient between fiber and matrix. To evaluate this effect, the [90/0] specimen was exposed to 2000 thermal cycles from 200 to 1000°F by cycling the specimen into and out of a furnace at a rate of 0.17 cycles/min. The test results are tabulated in Table 5 and are shown graphically in Fig. 10. They indicate that the thermal cycling had a negligible effect on the composite stiffness. The difference between as-received and heat-treated properties indicate that some damage may have been introduced during heat treatment, but the material was not significantly further damaged by the cyclic thermal load.

Further evidence to this effect was obtained by tensile testing several [0/90] specimens to failure. A typical specimen that had not been exposed to the thermal cycling had measured values of 22 Msi, 146 ksi, and 1.04% for the modulus, E_{11}, ultimate tensile strength, and failure strain, respectively, whereas an otherwise identical specimen had corresponding values of 21 Msi, 137 ksi, and 0.98% after being exposed to the cyclic thermal load. It should be pointed out that the thermal cycling conditions used in this study are fairly benign. The thermal cycling induces a few isolated matrix cracks, as well as some fiber/matrix debonding.[8] The current results indicate that neither the vibration analysis nor the tensile tests were

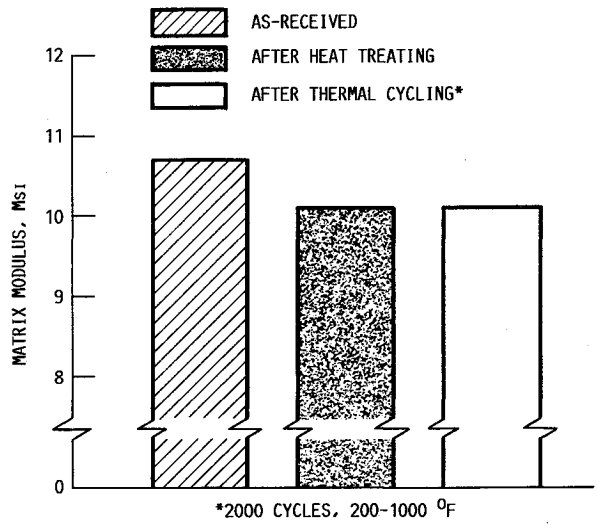

Fig. 10 Change in calculated matrix modulus for [90/0] specimen due to heat treatment and thermal cycling.

sufficient for detecting the limited amount of damage that occurred during thermal cycling.

Summary of Results

A combined experimental/analytical technique that uses the results of vibration testing together with finite element analysis was demonstrated and used to evaluate the degradation of mechanical properties of SiC/Ti-15-3 composites. The effects of heat treatment on specimens of varying ply orientation were analyzed, and representative results were presented that illustrate the effects of monotonic tensile loading, fatigue loading, and thermal cycling on composite stiffness.

The results for the five different ply orientations considered indicated that the effective in situ modulus of the matrix material in the as-received condition was an average of 15% lower than the monolithic value. In addition, the effect of heat treatment on the composite stiffness varied with the ply stacking sequence.

References

[1]Bahei-El-Din, Y. A., and Dvorak, G. J., "Plastic Deformation of a Laminated Plate with a Hole," *Journal of Applied Mechanics,* Vol. 47, No. 4, Dec. 1980, pp. 827–832.

[2]Lerch, B. A., Hull, D. R., and Leonhardt, T. A., "As-Received Microstructure of a SiC/Ti-15-3 Composite," NASA TM-100938, Aug. 1988.

[3]Lerch, B. A., Gabb, T. P., and MacKay, R. A., "Heat Treatment Study of the SiC/Ti-15-3 Composite System," NASA TP-2970, 2970, Jan. 1990.

[4]Jones, R. M, *Mechanics of Composite Materials,* Scripta, Washington, DC, 1975, pp. 85–146.

[5]Whitney, J. M., *Structural Analysis of Laminated Anistropic Materials,* Technomic, Lancaster, PA, 1987.

[6]MacNeal, R. H. (ed.), *The NASTRAN Theoretical Manual* (Level 15.5), MacNeal-Schwendler, Los Angeles, CA, 1972.

[7]Lerch, B. A., Private communication, NASA Lewis Research Center, Cleveland, OH.

[8]Lerch, B. A., "Damage Of a SiC/Ti-15V-3A1-3 δr-3Cr Composite due To Thermal Excursion," *HiTemp Review 1988,* NASA CP-10025, Nov. 1988, pp. 139–144.